Korean J. Chem. Eng., 36(3), 468-477 (2019)
DOI: 10.1007/s11814-018-0167-9

pISSN: 0256-1115
eISSN: 1975-7220

Influence of surfactant on the synthesis of $BiOCl/WO_3$ microcomposites for enhanced adsorption in aqueous solutions

Sangeeta Adhikari and Do-Heyoung Kim†

School of Chemical Engineering, Chonnam National University, 77 Yongbong-ro, Gwangju 61186, Korea
(*Received 16 August 2018 • accepted 24 October 2018*)

Abstract−$BiOCl/WO_3$ microcomposites were synthesized using a one-step hydrothermal route in the presence of a variety of surfactants: polyvinylpyrrolidone (PVP), triethylene glycol (TEG), and Triton X-100 (TX-100). The as-synthesized microcomposites were exploited as efficient adsorbents for removing organic dyes (rhodamine B and methylene blue). Prior to adsorption studies, the structural, functional, and morphological characteristics of these adsorbents were studied using analytical techniques, including XRD, FE-SEM, TEM, and UV-DRS, which revealed the presence of large surface areas. The experimental results show that the PVP-synthesized $BiOCl/WO_3$ microcomposite was significantly more effective as an adsorbent than the microcomposites synthesized using TEG or TX-100. This enhanced adsorption performance is attributable to the larger surface area associated with the developed microstructure of the PVP-stabilized $BiOCl/WO_3$ microcomposite. The $BiOCl/WO_3$ microcomposite synthesized from PVP was subjected to parametric studies involving catalyst dosage, pH, and initial dye concentration. The experimental data were fitted to isotherm models, and the mechanism of adsorption was investigated.

Keywords: $BiOCl/WO_3$ Composite, Surfactant, Adsorption, Rhodamine B, Methylene Blue

INTRODUCTION

Water contamination has become a serious global environmental concern, leading to the emergence of pollution-related lethal diseases [1]. The release of untreated effluents from industries, such as rubber, plastics, cosmetics, textiles, leather, paper, food, and mineral processing, contributes to the majority of wastewater pollution [2,3]. Most effluents include synthetic dye components that are extremely toxic, carcinogenic, and mutagenic; these pollutants can damage existing aquatic life and also pose serious ecological threats [4,5]. The use of aqueous based electrolytes is an emerging field in dye-sensitized solar cells due to its cost effectiveness and environmental friendliness due to absence of any toxic components [6-8]. Among the categories of synthetic dyes, those bearing azo/aryl and/or amino groups are recalcitrant because of their inherent xenobiotic properties and their potential resistance to microbial degradation [9,10]. Such contaminants are typically removed using existing methods which include membrane separation, adsorption, oxidation, and coagulation, as well as treatment with biological microbes [11-14]. There are also studies which report derivation of photosensitizer from waste for visible light degradation of potential contaminants like monochlorophenols [15]. Adsorption has been reported to be cost-effective for the removal of micro-contaminants from aqueous media [16,17]. Nanomaterials have captured the interest of researchers because of their surface-active properties, and because their structures can be easily tuned for wastewater-treatment applications [18-20].

Multicomponent bismuth oxyhalides, typically BiOCl, are important ternary compounds with excellent optical, catalytic, luminescent, electrical, and magnetic properties [21,22]. The wide band gap of BiOCl (~3.4 eV) does not facilitate its use in a single-component system; rather, it is surface modified by doping, composite formation, and adding co-catalysts [23,24]. On the other hand, although the lamellar structure of BiOCl is quite popular for use in photocatalytic processes, the reported adsorption capacities of BiOCl are comparatively low [22,24]. Improving the adsorption capacity of BiOCl remains a challenge; combining two characteristic materials to form a composite adsorbent is a useful strategy [25,26]. In this context, WO_3 is another semiconductor that has widely been studied for optoelectrical, sensing, and catalytic applications [27-29]. The $BiOCl/WO_3$ combination has been used as an efficient visible-light photoactive catalyst for the degradation of dyes [30]; however, to the best of our information, there are no studies on the adsorption properties of this composite.

Nanomaterials are known for their unique physicochemical properties that are dimension dependent [31]. A convenient and cost-effective way to control the sizes of these materials uses soft templates, such as surfactants [32,33]. The anisotropic growth of a material in the presence of a surfactant is an interesting subject of composite research. In this regard, the current work was carried out by the hydrothermal synthesis of the $BiOCl/WO_3$ composite, as an adsorbent, with a variety of surfactants, namely polyvinylpyrrolidone, triethylene glycol and Triton X-100. The effect of the individual surfactant on composite morphology and phase formation was explored. Adsorption performance against cationic dyes, namely rhodamine B and methylene blue, was also investigated. The composite adsorbent was optimized through a detailed parametric study, after which kinetics and isotherm modeling were carried out.

†To whom correspondence should be addressed.
E-mail: kdhh@chonnam.ac.kr

MATERIALS AND METHODS

All chemicals were procured from Sigma Aldrich and used without any further purification.

1. BiOCl-WO_3 Microcomposites Synthesized with Different Surfactants

In a typical BiOCl-WO_3-microcomposite synthesis process, a stoichiometric amount of sodium tungstate dihydrate ($Na_2WO_4 \cdot 2H_2O$) was dissolved in 20 mL of deionized water to produce a clear solution. The predetermined amount of surfactant (polyvinylpyrrolidone (PVP), triethylene glycol (TEG), or Triton X-100 (TX-100)) was added to the solution, after which it was magnetically stirred until a colorless solution was obtained. The solution of surfactant and sodium tungstate was added slowly to a 20 mL aliquot of a solution of bismuth nitrate pentahydrate ($Bi(NO_3)_3 \cdot 5H_2O$), prepared in a separate beaker. A stoichiometric amount of NaCl crystals was added to the resultant solution, and the mixture was stirred for 2 h. The homogeneous mixture was then poured in a 60 mL Teflon beaker and sealed in a Teflon-lined stainless-steel reactor. The mixture was autoclaved at 180 °C for 24 h and then allowed to cool naturally. The precipitate obtained following the hydrothermal reaction was collected by filtration, and washed with water and isopropanol to obtain the final product free of the surfactant. The collected product (on the filter paper) was dried overnight in a hot-air oven at 60 °C. In a similar manner, BiOCl powder was prepared using PVP as the surfactant without the addition of sodium tungstate to the reaction mixture.

2. Characterizing the Adsorbents

The as-synthesized dried adsorbents were characterized for their structural, functional, and morphological properties, as well as their surface charges using a variety of analytical techniques. A power X-ray diffraction pattern was acquired for each adsorbent using a PANalytical X-ray diffractometer with Cu Kα radiation. Adsorbent morphologies were examined by field-emission scanning electron microscopy (FESEM, JEOL JSM-7500F). The adsorbents were further examined by high-resolution transmission electron microscopy (HRTEM, TECNAI G2 F20). FTIR spectra of the as-synthesized adsorbents were acquired using a Bruker Vertex 80v FT-IR/Raman spectrophotometer fitted with a reflection ATR (attenuated total reflectance) unit. FT-IR spectra were acquired in the 450-4,000 cm^{-1} range. A Varian Cary spectrophotometer was used to acquire UV-vis absorbance spectra of the synthesized adsorbents. Nitrogen adsorption-desorption isotherms of the optimized adsorbent were obtained using a Micromeritics ASAP2010 surface-area analyzer.

3. Batch Studies

Adsorption studies involved a series of batch experiments. Cationic rhodamine B (RB) and methylene blue (MB) were used as model pollutants in the adsorption studies. A 1- mg/L standard stock solution was prepared for each dye solution. Batch adsorption experiments were performed with 30 mL of the dye solution in a 50 mL beaker covered with aluminum foil to avoid contamination by foreign particles. All batch experiments were at room temperature (27±2 °C), with amounts of adsorbent in solution that ranged from 5 to 60 mg. To maintain homogeneous mixing of the dye solution and the adsorbent, the suspension was magnetically stirred at 500 rpm. Solutions of 0.1 M HCl and 0.1 M NaOH were used for adjusting pH of the solution to between 2 and 12 during the pH studies. At specific times during the experiment, aliquots were removed from the solution and separated by centrifugation to obtain the dye solution devoid of adsorbent particles. The as-obtained dye solution was subjected to UV-vis spectrophotometry to determine the absorbance at the characteristic wavelength maxima (λ_{max}) for rhodamine B (554 nm) and methylene blue (664 nm). Absorbance was converted into dye concentration using the Beer-Lambert law. The adsorption percentage was calculated using the following equation:

$$\% \text{ Dye Adsorption} = \frac{(C_o - C)}{C_o} \times 100 \quad (1)$$

where C_o (mg/L) and C (mg/L) are the initial and final concentrations of the dye solution following adsorption for the specified time. Parametric adsorption studies were carried out using a similar process. The amount of dye adsorbed per gram of adsorbent was calculated using the following equation:

$$q_e = \frac{(C_o - C) \times V}{m} \quad (2)$$

where q_e (mg/g) presents the amount of dye adsorbed by the adsorbent; V (mL) presents the volume of the dye solution; and m (g) is the amount of adsorbent used during the adsorption study.

RESULTS AND DISCUSSION

1. Characterizing the Materials

1-1. Crystal Structure Analyses

The phases and corresponding crystal structures of the as-syn-

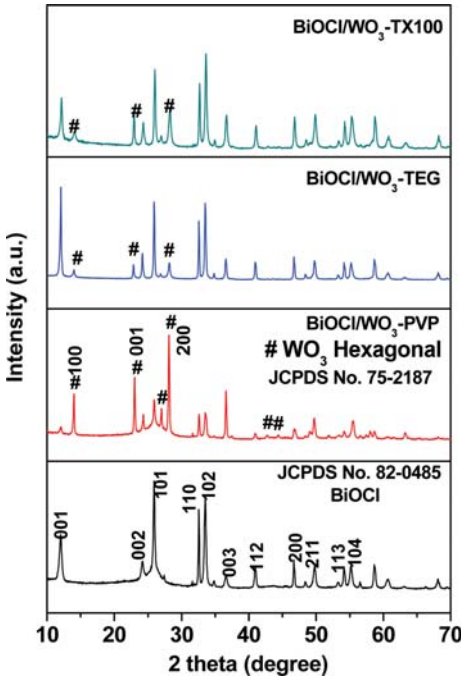

Fig. 1. XRD patterns of the as-synthesized BiOCl, and the BiOCl/WO_3-PVP, BiOCl/WO_3-TEG, and BiOCl/WO_3-TX100 composites.

thesized nanocomposite adsorbents were examined by XRD, as shown in Fig. 1. The BiOCl/WO_3 nanocomposites synthesized using PVP, TEG, and TX-100 are referred to as "BiOCl/WO_3-PVP," "BiOCl/WO_3-TEG," and "BiOCl/WO_3-TX100," respectively, with the pristine BiOCl synthesized in the presence of PVP simply referred to as "BiOCl." The XRD pattern of pristine BiOCl is well indexed to JCPDS No. 82-0485, and corresponds to the tetragonal crystal structure of BiOCl in the P4/nmm space group; all observed peaks correspond to those of the standard, and no impurity peaks were observed, suggesting that the synthesized BiOCl is of high purity. The peak of highest intensity corresponds to the (101) plane of BiOCl. The BiOCl/WO_3 composite synthesized using PVP displays an XRD pattern that appears to be a mixture of those of the two constituents, confirming the presence of both the tetragonal and hexagonal crystal structures of BiOCl and WO_3. The high-intensity peaks in the pattern of BiOCl/WO_3-PVP are indexed to hexagonal WO_3 (JCPDS No. 75-2187). The XRD peaks observed for WO_3 are consistent with high crystallinity; it appears that the WO_3 is not influenced by the presence of the PVP. However, the composite synthesized using TEG shows a sharp decline in the intensity of the peak corresponding to the (200) plane of hexagonal WO_3, which demonstrates that TEG significantly impacts the formation of the WO_3 crystal phase. Similarly, the presence of TX100 was also observed to affect the crystal phase; it appears that the (001) and (200) planes of hexagonal WO_3 have attempted to grow simultaneously with the BiOCl crystal planes. Despite this, the high crystallinity of BiOCl dominates the hexagonal WO_3. Both of the composites synthesized using TEG and TX-100 exhibit dominant BiOCl. Apart from BiOCl and WO_3, no other phases were observed, which verifies that the composites are pure. Since each surfactant influences both the BiOCl and WO_3 phases, the morphologies and functional groups of the as-synthesized BiOCl/WO_3 composites

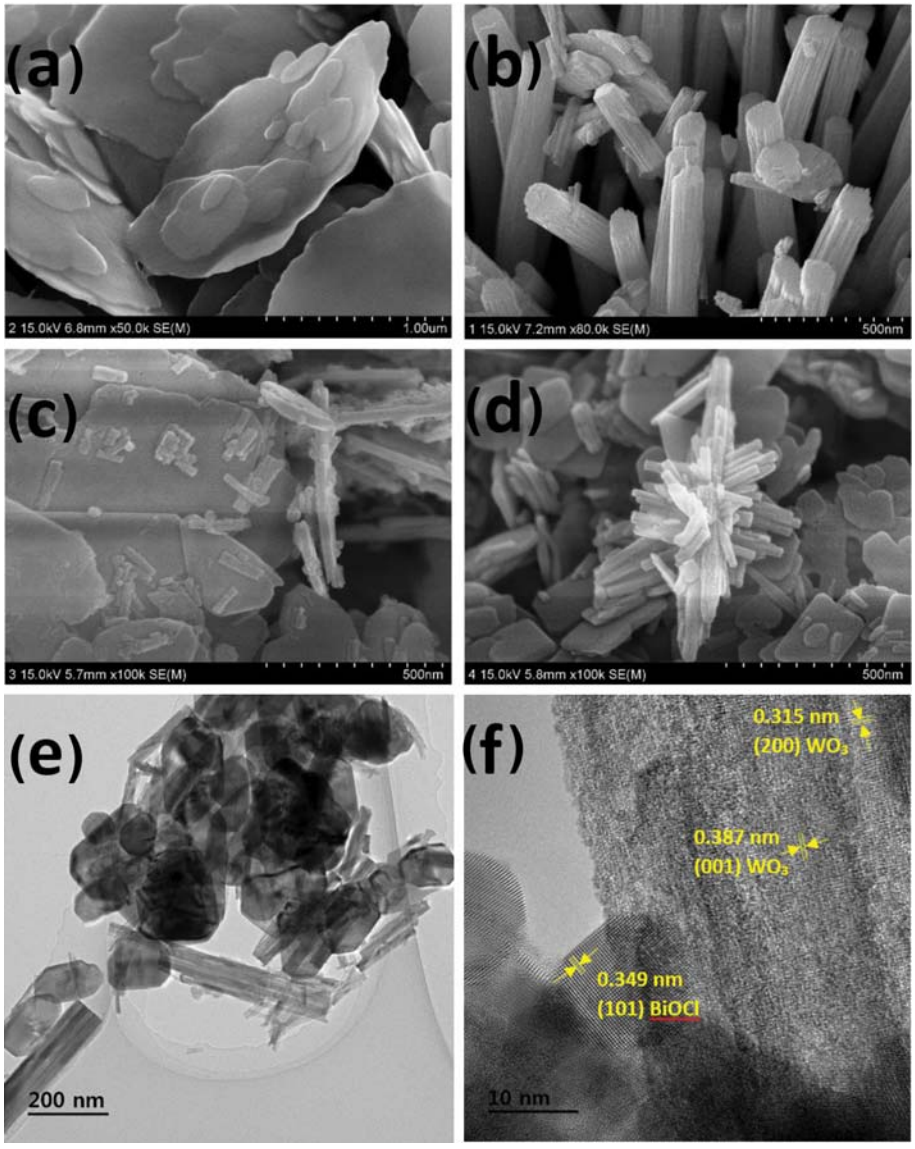

Fig. 2. FESEM images of the as-synthesized (a) BiOCl; (b) BiOCl-WO_3-PVP; (c) BiOCl-WO_3-TEG; (d) BiOCl-WO_3-TX100; (e) TEM image (inset shows the SAED pattern) and (f) HRTEM image of the as-synthesized BiOCl-WO_3-PVP.

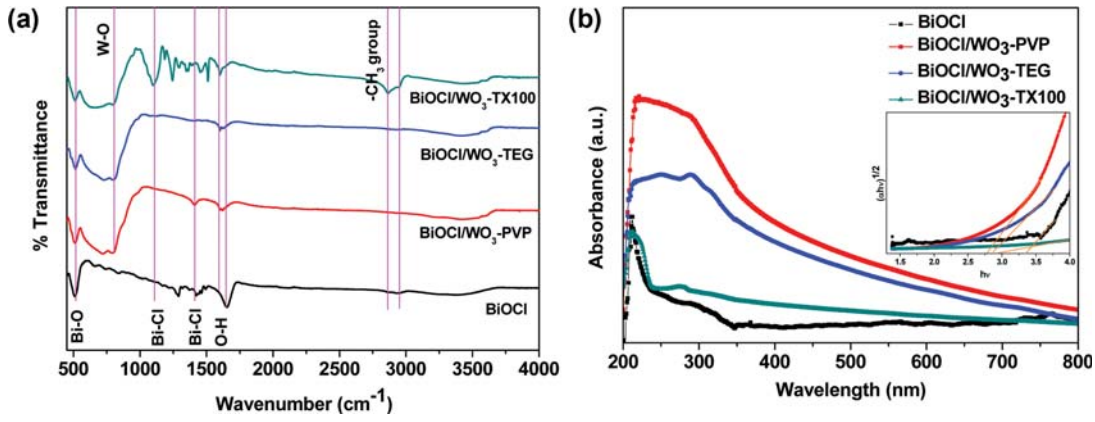

Fig. 3. (a) FTIR and (b) UV-Vis absorbance spectra of the as-synthesized adsorbents.

were examined to understand the impact of each surfactant.

1-2. Morphological Analyses

FESEM and HRTEM were used to investigate the influence of the surfactant on morphology, the results of which are shown in Fig. 2(a)-(f). The as-synthesized BiOCl, formed in the presence of PVP, is composed of ultrathin irregular disks that are 200 nm to 2.5 micron in size, and about 8-10 nm thick (Fig. 2(a)). On the other hand, the $BiOCl/WO_3$-PVP composite has a significantly different morphology (Fig. 2(b)) where, in addition to disk-like structures, nanofibers with diameters of about 130-140 nm are observed. Furthermore, the disk sizes are also smaller as a result of the growth of the fiber-like structures that correspond to hexagonal WO_3. The formation of such WO_3-fiber-like structures in the presence of NaCl has been reported elsewhere [34]. It has also been reported that BiOBr, which also exhibits a similar structure, absorbs PVP specifically and selectively onto its (001) plane to form an anisotropic structure, whereas the (001) plane exhibits the most intense reflection in the absence of PVP [35]. Since the (001) plane of BiOCl corresponds to the fourth-most intense peak in the present case, we conclude that BiOCl behaves in a similar manner to BiOBr; PVP adsorbs onto this plane, which facilitates the growth of the (101) plane. The most intense peak in the XRD pattern of the $BiOCl/WO_3$-TEG composite corresponds to the (001) plane of BiOCl; hence TEG is preferentially adsorbed onto the planes of the hexagonal WO_3 that correspond to the most intense signals, thereby hindering their growth. This observation provides further evidence in favor of PVP adsorption to the (001) plane of BiOCl. As a result, $BiOCl/WO_3$-TEG displays a morphology that is a mixture of irregular disks and small rods, as seen in Fig. 2(c). Shearing is suppressed during the formation of the fiber structures in the presence of TEG in the reaction solution. The WO_3 rods in the $BiOCl/WO_3$-TEG composite are about 120-125 nm long, with diameters of around 25-30 nm. On the other hand, the $BiOCl/WO_3$-TX100 structure is composed of a mixture of ultrathin disks and aggregated rod-like structure, as well as flower structures formed through the self-assembly of small WO_3 rods (Fig. 2(d)). The individual disks are much smaller than the BiOCl disks, which is attributed to TX-100 affecting rod growth while inhibiting the growth of BiOCl disks through adsorption onto a specific plane. The XRD pattern of $BiOCl/WO_3$-TX100 shows a significantly more intense reflection from the (102) plane of BiOCl, compared to pristine BiOCl, with lower-intensity peaks for the (001) and (101) planes, which are among the most-intense peaks in the XRD pattern of BiOCl. These analyses reveal that the surfactants influence the morphology in remarkable ways, a consequence of their adsorptions to specific planes during the hydrothermal reaction, which affects the growth of the various crystal planes. As $BiOCl/WO_3$-PVP exhibited the strongest adsorption properties, its high-resolution characteristics are detailed in Fig. 2(e)-(f). Fig. 2(e) clearly shows variations in the sizes of the ultrathin irregular disks, as well as the fiber morphology. The fibers appear to be broken because of ultrasonication during sample preparation. The calculated lattice fringes (Fig. 2(f)) are 0.349, 0.315, and 0.387 nm, which correspond to the (101) plane of BiOCl, and the (200) and (001) planes of WO_3, respectively. These values are well matched to the XRD data for the $BiOCl/WO_3$-PVP composite.

1-3. Functional-group and Optical Analyses

The functional groups of the as-synthesized BiOCl and $BiOCl/WO_3$ composites prepared using different surfactant were analyzed by FT-IR spectroscopy. The FTIR spectrum of pristine BiOCl (Fig. 3(a)) displays absorption peaks at 516 (Bi-O symmetrical stretch), 1,095, 1,918 (Bi-Cl), and 1,642 cm^{-1} (O-H) [23,36]. An additional peak at 785 cm^{-1} is evident in the spectra of the various $BiOCl/WO_3$ composites, which corresponds to W-O-W bending and confirms the presence of WO_3 in the composite adsorbent [37]. A band at 1,592 cm^{-1} that corresponds to additional hydroxyl groups is observed in the spectra of the adsorbents synthesized using PVP and TEG. The $BiOCl/WO_3$-TX100 composite exhibited peaks between 2,500 and 3,000 cm^{-1} that correspond to the $-CH_3$ groups in TX-100, and below 1,500 cm^{-1} that correspond to $-CH_2-$ and -OH vibrations [38].

The optical properties of pure BiOCl and the surfactant-synthesized $BiOCl/WO_3$ composites were examined by UV-Vis diffuse reflectance spectroscopy (DRS), and the corresponding DRS spectra are displayed in Fig. 3(b). An increase in absorption intensity was observed when the WO_3 semiconductor was present in the composite, since it has a narrower band gap than BiOCl. Shifts in the absorption wavelengths of the WO_3-containing composites, compared to pristine BiOCl, were observed, and the high absorbance exhibited by $BiOCl/WO_3$-PVP is due to the dominance of WO_3 in the composite. The inset in Fig. 3(b) shows Tauc plots of

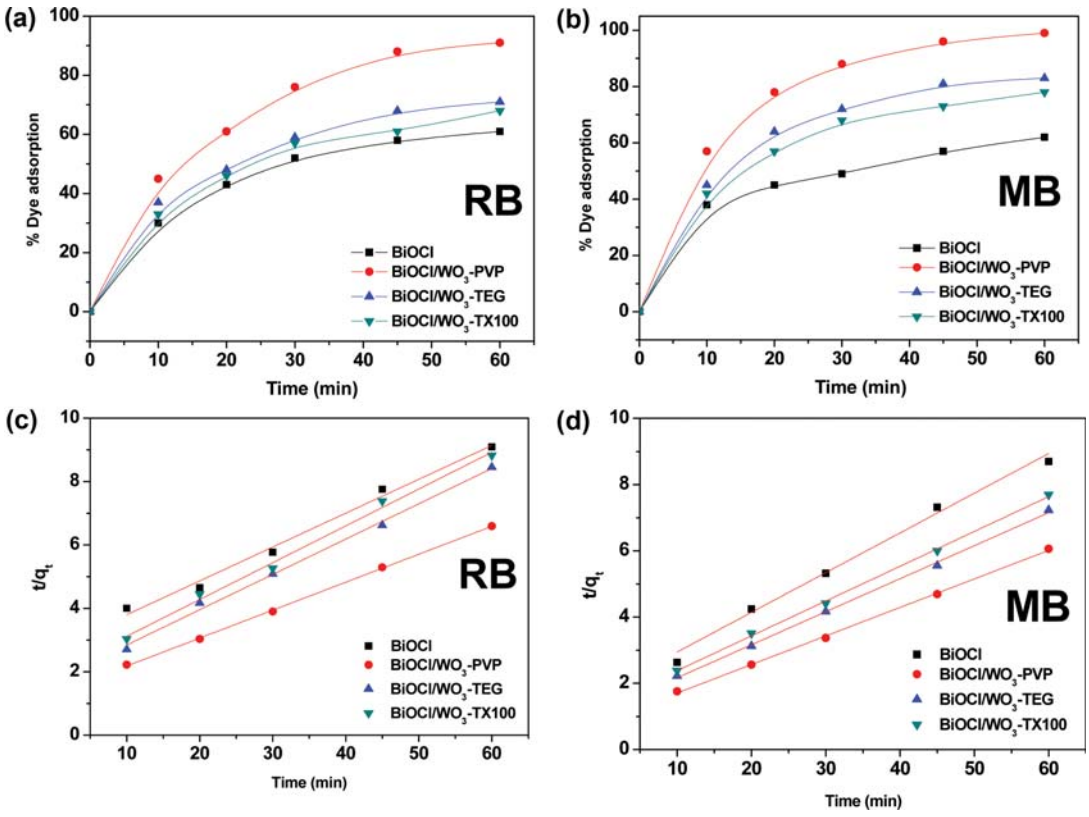

Fig. 4. Adsorption and pseudo-second-order kinetics data for the various as-synthesized adsorbents: (a), (c) Rhodamine B and (b), (d) methylene blue (dye concentration, 10 mg/L; adsorbent concentration, 1 mg/mL (30 mg/30 mL)).

$h\nu$ versus $(\alpha h\nu)^{1/2}$; extrapolating these plots provides the band gaps of the various composites, which are 3.35, 2.75, 2.83, and 2.91 eV for BiOCl, BiOCl/WO_3-PVP, BiOCl/WO_3-TEG, and BiOCl/WO_3-TX100, respectively. Similar values have been reported in the literature [39,40].

1-4. Preliminary Adsorption and Kinetics Studies

Preliminary adsorption studies were performed with 30 mL of a solution of rhodamine B (RB) or methylene blue (MB), and 30 mg of the adsorbent at room temperature. The effect of contact time on the adsorption properties of BiOCl, BiOCl/WO_3-PVP, BiOCl/WO_3-TEG, and BiOCl/WO_3-TX100 toward RB and MB was studied, the results of which are displayed in Figs. 4(a) and 4(b), respectively. Among the as-synthesized adsorbents, BiOCl/WO_3-PVP exhibited enhanced adsorption, which is attributable to the presence of both ultrathin disks and the one-dimensional fiber-like structures of BiOCl and WO_3, respectively. The adsorption percentage for RB shown by BiOCl is closer to that of the TEG- and TX-100-synthesized BiOCl/WO_3 composites. However, BiOCl showed a significant difference in its ability to adsorb MB compared to the composite adsorbents. BiOCl/WO_3-TEG adsorbed less RB and MB than the BiOCl/WO_3-TX-100 composite, which is attributed to the morphological differences between the adsorbents prepared in the presence of the two surfactants. The BiOCl/WO_3-TX100 adsorbent tended to agglomerate, due its small disks and rods, to form flowers that reduced the number of active sites for adsorption. However, the disks in the BiOCl/WO_3-TEG sample were larger than those of the TX-100-synthesized composite, and the additional active sites facilitated adsorption. The percentage of adsorbed RB was observed to gradually increase with time, whereas more than 90% of the MB was adsorbed in 30 min. The fast and significant adsorption of MB is attributed to its smaller structure compared to RB. Methylene blue was completely adsorbed within 60 min by BiOCl/WO_3-PVP, whereas over 90% of the RB was adsorbed within 60 min. No further changes in adsorption were observed after 60 min.

This adsorption behavior is better understood through kinetics studies that shed light on the adsorption mechanism involving the synthesized adsorbents. The experimental RB- and MB-adsorption data were fitted to pseudo-first-order and pseudo-second-order kinetics models; these first-order and second-order models are governed by their respective integrated equations, as given below [41,42]:

$$\mathrm{Log}(q_e - q_t) = \mathrm{Log}q_e - k_1\left(\frac{t}{2.303}\right) \quad (3)$$

and

$$\frac{t}{q_t} = \frac{1}{k_2 q_e^2} + \frac{1}{q_e}t \quad (4)$$

where q_e is the amount of dye adsorbed at equilibrium (mg/g), q_t is the amount of dye adsorbed at time t (mg/g), k_1 is the first-order kinetic rate constant (min^{-1}), and k_2 is the second-order rate constant in (g mg^{-1} min^{-1}).

The kinetic data obtained by kinetics-model fitting are summarized in Table 1, which includes rate constants, the amounts of ad-

Table 1. Kinetic data for the adsorption of RB and MB by different adsorbents according to pseudo-first-order and pseudo-second-order models

Rhodamine B		Pseudo-first-order kinetics			Pseudo-second-order kinetics		
Adsorbent	$q_{e,exp}$	k_1 (min^{-1})	$q_{e,cal}$ (mg g^{-1})	R^2	k_1 (g mg^{-1} min^{-1})	$q_{e,cal}$ (mg /g)	R^2
BiOCl	6.6	0.038	4.64	0.971	4.23×10^{-3}	9.4	0.995
$BiOCl/WO_3$-PVP	9.1	0.046	7.04	0.985	7.00×10^{-3}	11.3	0.999
$BiOCl$-WO_3-TEG	7.1	0.067	7.55	0.991	6.90×10^{-3}	8.9	0.996
$BiOCl$-WO_3-TX100	6.8	0.051	6.14	0.990	6.85×10^{-3}	8.6	0.996
Methylene blue							
BiOCl	6.2	0.051	5.15	0.962	8.06×10^{-3}	8.3	0.999
$BiOCl/WO_3$-PVP	9.9	0.075	9.6	0.991	8.72×10^{-3}	11.6	0.999
$BiOCl$-WO_3-TEG	8.3	0.071	8.9	0.981	8.58×10^{-3}	10.2	0.999
$BiOCl$-WO_3-TX100	7.8	0.061	7.1	0.993	8.30×10^{-3}	9.5	0.999

sorbed dye at equilibrium (both experimental and calculated by each model), and the coefficients of determination; the best kinetic model corresponds to that with the highest coefficient of determination. Inspection of Table 1 reveals that the pseudo-first-order model exhibits the poorer correlation. On the other hand, the experimental data for RB and MB are well modeled by pseudo-second-order kinetics, with coefficients of determination in excess of 0.99, as shown in Figs. 4(c) and 4(d), respectively. The present study also reveals that the $BiOCl/WO_3$-PVP composite adsorbent is associated with a high rate constant. Hence, further parametric studies involving both dyes were performed with the $BiOCl/WO_3$-PVP composite.

1-5. The Effects of the amount of Adsorbent and pH

Since adsorption efficiency depends on the amount of adsorbent added to the dye solution, a series of adsorption experiments were carried out with the $BiOCl/WO_3$-PVP composite as adsorbent, and 30 mL samples of RB and MB at concentrations of 10 mg/L. Adsorption experiments were carried out at room temperature for up to 60 min, and the results of experiments in which the amount of adsorbent was varied between 5 and 60 mg are displayed in Fig. 5(a). The results reveal that both dyes are gradually more adsorbed with increasing amounts of adsorbent. In the case of RB, complete dye adsorption is achieved with 60 mg of the adsorbent, whereas 30 mg is sufficient to adsorb MB at a concentration of 10 mg/L;

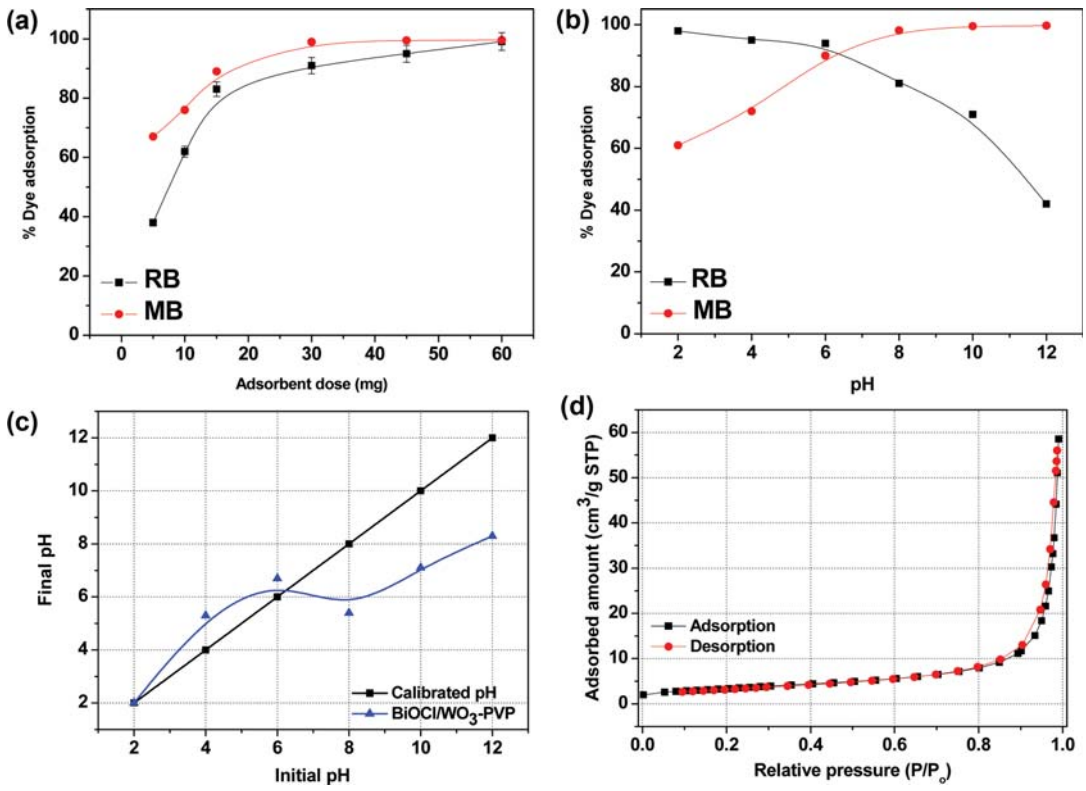

Fig. 5. Studies on the effect (a) of adsorbent dose and (b) pH. (c) pH drift study, and (d) BET isotherm for $BiOCl/WO_3$-PVP.

however, adsorbent doses above 30 mg have little effect on the adsorption percentage. Given that MB achieved equilibrium with 30 mg of the adsorbent, this amount of adsorbent was used in further parametric studies.

The effect of the pH of the dye solution (pH 2 to 12) on adsorption efficiency was investigated with 30 mL of dye solution containing 30 mg of adsorbent at room temperature over 60 min; the results of which are shown in Fig. 5(b). The percentage of adsorbed methylene blue increased from 60 to 100% with increasing solution pH, and was observed to equilibrate at pH 8. On the other hand, rhodamine B exhibited a significant decrease in adsorption percentage with increasing pH of the (dye and adsorbent) suspension. This deteriorating adsorption performance was likely due to structural changes undergone by rhodamine B in acidic and basic media. The carboxylate group in rhodamine B is negatively charged in acidic media and adsorbs onto the adsorbent through electrostatic attraction. On the other hand, the adsorbent surface is negatively charged which, under basic conditions, reduces adsorption. The adsorption of methylene blue is favored under basic conditions due to electrostatic interactions between the negatively surface charge of the adsorbent and the positive charge of N-ethyl group of MB. The tungsten surface finishes its coordination shells with the existing OH and NH groups. As the pH is varied, these groups can further participate in binding or release of H^+, resulting in a surface that is either positively or negatively charged due to these reactions. The pH-dependent behavior exhibited by RB and MB has also been observed by other researchers [2,43,44].

The surface-charge characteristics of the optimized BiOCl/WO_3-PVP adsorbent were examined by evaluating the point of zero charge (PZC) using the standard pH-drift method, as reported elsewhere [45,46]. The PZC is representative of the surface acidity of the adsorbent and can explain the adsorption behavior of a dye at a surface. Various aqueous solutions were prepared using of 0.01 M HCl and 0.01 M NaOH such that the pH values were between 2 to 12. A 20-mg sample of the adsorbent was added to about 20 mL of each solution, followed by ultrasonication to ensure that the adsorbent was homogeneously distributed. The solutions were aged for 24 h at room temperature, and the final pH of the solution was measured. Plots of calibrated pH and final pH as functions of initial pH are in Fig. 5(c). The intersection point, where the final-pH and calibrated-pH curved cross, is the PZC of the adsorbent, which was determined to be 6.2. The surface of the BiOCl/WO_3-PVP adsorbent is predominately negatively charged above the PZC, which reveals that near neutral pH favors the adsorption of the dye due to the negative adsorbent's surface charge. The surface area of the adsorbent also plays a crucial role in determining adsorption performance. The specific surface area of the optimized BiOCl/WO_3-PVP composite was determined by the Brunauer-Emmett-Teller (BET) method; the corresponding nitrogen adsorption-desorption isotherms are in Fig. 5(d). The calculated active surface

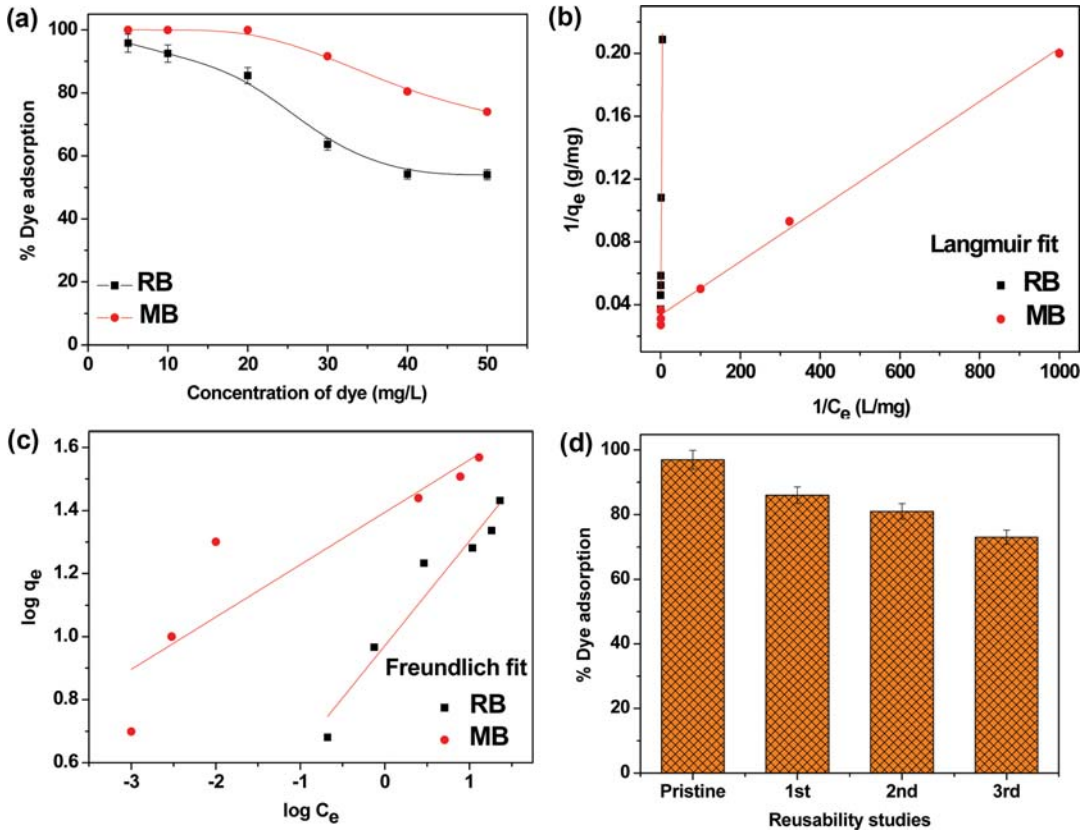

Fig. 6. (a) RB and MB adsorption percentages as functions of initial dye concentration; (b) Langmuir adsorption isotherm ($1/C_e$ vs. $1/q_e$); (c) Freundlich adsorption isotherm (log C_e vs. log q_e) (adsorbent, BiOCl/WO_3-PVP; adsorbent concentration, 1 mg/mL (30 mg/30 mL of aqueous dye solution); and (d) reusability studies with methylene blue (initial concentration, 10 mg/L).

area of the adsorbent was determined to be 13.12 m^2/g (based on the N_2-adsorption data), which is similar to previously reported surface areas [30,47].

1-6. Adsorption Isotherms

The adsorption of aqueous dye solutions onto the optimized $BiOCl/WO_3$-PVP composite was studied by varying the initial dye concentration at an adsorbent concentration of 1 mg/mL (30 mg of adsorbent in 30 mL of the dye solution). Each batch experiment was carried out for 60 min, the results of which are in Fig. 6(a). Adsorption performance was observed to improve with increasing concentration because the active adsorption sites tend to saturate due to the high concentration of the adsorbate and the fixed amount of the adsorbent in these batch experiments. However, adsorption tended to gradually decrease at concentrations above 20 mg/L for each dye, and was almost saturated above 40 mg/L. Furthermore, the adsorption data were fitted to the Langmuir and Freundlich isotherms to explore the relationship between adsorbate concentration and the equilibrium behavior of the adsorbed dye [48]. These models provide the maximum adsorption capacity, in which the Langmuir model assumes saturated monolayer coverage of adsorbate molecules onto the adsorbent surface, while the Freundlich model assumes multilayer adsorption [49]. The linear form of the Langmuir equation is given by:

$$\frac{1}{q_e} = \frac{1}{q_o b C_e} + \frac{1}{q_o} \tag{5}$$

where, q_e represents the amount of dye adsorbed at equilibrium (mg/g), C_e is the equilibrium adsorbate concentration (mg/L), q_o represents the monolayer adsorption capacity (mg/g), and b is the Langmuir constant, otherwise known as the binding-energy constant. The relationship between $1/C_e$ and $1/q_e$ is shown in Fig. 6(b).

The linear form of the Freundlich isotherm is given by [49]:

$$\mathrm{Log} q_e = \mathrm{Log} K_f + 1/n \log C_e \tag{6}$$

where q_e and C_e are as defined above, K_f is the Freundlich adsorption constant (L/g), and 1/n is the adsorption intensity. The data obtained through parametric fitting to the above-mentioned isotherms (Fig. 6(c)) are listed in Table 2, which clearly reveals that the experimental data for both RB and MB are best fitted to the Langmuir adsorption isotherm, with coefficients of determination close to unity when the $BiOCl/WO_3$-PVP composite was used as the adsorbent. The Langmuir-model-determined maximum adsorption capacity of $BiOCl/WO_3$-PVP toward rhodamine B and methylene blue is 21.50 and 29.85 mg/g, respectively.

The reusability of the adsorbent is of great importance for batch adsorption processes. Reusability experiments were carried out by separating the adsorbent from the adsorbate solution by centrifugation followed by drying at 90 °C in a hot-air oven following adsorption at an initial dye concentration of 10 mg/L and an adsorbent concentration of 1 mg/mL (30 mg/30 mL); methylene blue was the chosen dye, and the optimized $BiOCl/WO_3$-PVP composite was used as the adsorbent during these experiments. After the first adsorption experiment, the adsorbent was reused three more times. The adsorption percentage was observed to degrade; however, the difference between the first and third runs was only approximately 8%. This decrease is attributed to particle agglomeration and the occupancy of some sites by the dye adsorbed by the $BiOCl/WO_3$-PVP composite. The difference in adsorption percentage is not significant, which indicates that the adsorbent recycles well.

Table 2. Langmuir and Freundlich isotherm data for the adsorptions of RB and MB to the $BiOCl/WO_3$-PVP composite

Dye	Langmuir parameter			Freundlich parameter		
	q_o (mg/g)	b (L/mg)	R^2	K_f (mg/g)	n	R^2
RB	21.50	1.33	0.98	9.36	3.11	0.94
MB	29.85	167.5	0.99	24.78	6.02	0.82

1-7. Dye Adsorption Mechanism

Knowledge of the mechanism of an adsorption-centered removal technique is important for the approval of the process; it also provides an understanding of the chemical nature of the adsorbent material, which is helpful when designing and improving adsorbents for future applications. In general, the adsorbent surface is the most important feature; adsorption behavior can be quite complex and depends on the nature of the dye. On the basis of the experimental results obtained in this study, separate three-step mechanisms have been tentatively proposed for the adsorptions of rhodamine B and methylene blue (MB) by the $BiOCl/WO_3$ composite. The $BiOCl/WO_3$-PVP composite material acts as a double agent, depending on the pH, which benefits the removal of the desired contaminant. In the first stage, electrostatic attraction due to charge polarization facilitates the adsorption of dye molecules onto the surface of the adsorbent. The second step involves interactions of the dye molecules with the available pores in the adsorbent through intra-particle diffusion, while the third (equilibrium or overlapping) stage occurs when dye molecules occupy all of the available sites and additional dye molecules begin to overlap with other another molecules, resulting in reduced adsorption capacity. As mentioned, the material acts as a double agent because variations in pH result in the efficient removal of the dye from the solution. Hence, the uptake of RB and MB may be due to proton-transfer mechanisms in the first step, which is a result of the acidic/basic nature of the material, which is sensitive to changes in pH and affects its ability to adsorb the organic molecule and form a stable complex. A schematic representation of the dye-adsorption mechanism is shown in Fig. 7. The adsorbent surface sites are predominately negatively charged under neutral conditions; therefore, they electrostatically attract methylene blue and rhodamine. The adsorption efficiency of MB is slightly lower than that of RB, since the latter is advantaged by the coexistence and competition of both the positive and negative sites of RB at high pH.

CONCLUSIONS

$BiOCl/WO_3$ composite adsorbents were synthesized using a simple, facile, and inexpensive hydrothermal technique in the presence of a variety of surfactants, including polyvinylpyrrolidone, triethylene glycol, and Triton X-100. A surfactant significantly influences the morphology of the adsorbent, due to specific planar adsorptions that affect the growths of the crystal planes of the adsorbent. The $BiOCl/WO_3$-PVP composite exhibited the best adsorp-

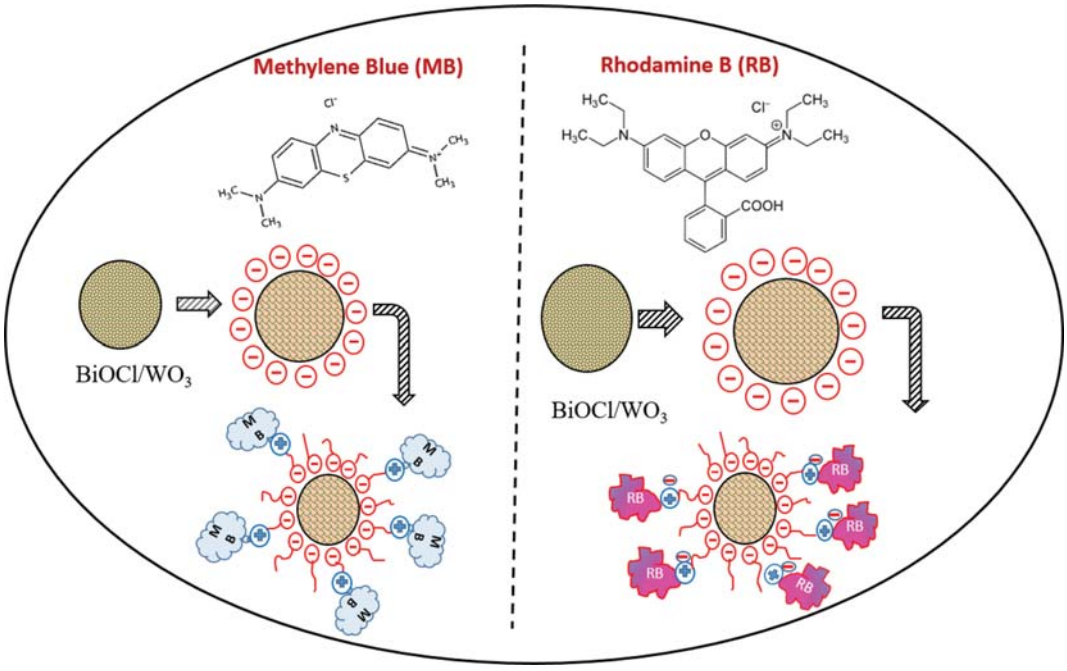

Fig. 7. Proposed dye-adsorption mechanism involving the BiOCl/WO_3-PVP composite.

tion performance for both rhodamine B and methylene blue, with the highest adsorption capacity of 21.50 and 29.85 mg/g, respectively. The adsorption processes followed pseudo-second-order kinetics and were well fitted by the Langmuir isotherm model. In addition, the as-synthesized BiOCl/WO_3-PVP adsorbent exhibited good recyclability, even after three consecutive batch adsorption process.

ACKNOWLEDGEMENT

The authors would like to thank the National Research Foundation of Korea (NRF-2015M3A7B 4050 424) for research support. We also thank the Korea Basic Science Institute (KBSI) at Gwangju Center for the analysis.

REFERENCES

1. A. Srinivasan and T. Viraraghavan, *J. Environ. Manage.*, **91**, 1915 (2010).
2. M. A. M. Salleh, D. K. Mahmoud, W. A. W. A. Karim and A. Idris, *Desalination*, **280**, 1 (2011).
3. G. Bayramoglu and M. Y. Arica, *Korean J. Chem. Eng.*, **35**, 1303 (2018).
4. S. Khamparia and D. Jaspal, *J. Environ. Manage.*, **183**, 786 (2016).
5. N. P. Raval, P. U. Shah and N. K. Shah, *Environ. Sci. Pollut. Res. Int.*, **23**, 14810 (2016).
6. S. Galliano, F. Bella, G. Piana, G. Giacona, G. Viscardi, C. Gerbaldi, M. Grätzel and C. Barolo, *Sol. Energy*, **163**, 251 (2018).
7. F. Bella, S. Galliano, C. Gerbaldi and G. Viscardi, *Energies*, **9**, 384 (2016).
8. F. Bella, S. Galliano, M. Falco, G. Viscardi, C. Barolo, M. Grätzel and C. Gerbaldi, *Chem. Sci.*, **7**, 4880 (2016).
9. H. N. Park, C.-W. Cho, H. A. Choi and S. W. Won, *Korean J. Chem. Eng.*, **34**, 2519 (2017).
10. M. Zhu, W. Tian, H. Chai and J. Yao, *Korean J. Chem. Eng.*, **34**, 1073 (2017).
11. J. Sojka-Ledakowicz, R. Zylla, Z. Mrozinska, K. Pazdzior, A. Klepacz-Smolka and S. Ledakowicz, *Desalination*, **250**, 634 (2010).
12. S. K. Ling, S. Wang and Y. Peng, *J. Hazard. Mater.*, **178**, 385 (2010).
13. A. Pirkarami and M. E. Olya, *J. Saudi Chem. Soc.*, **21**, S179 (2017).
14. C. R. Holkar, A. J. Jadhav, D. V. Pinjari, N. M. Mahamuni and A. B. Pandit, *J. Environ. Manage.*, **182**, 351 (2016).
15. P. Avetta, F. Bella, A. Bianco Prevot, E. Laurenti, E. Montoneri, A. Arques and L. Carlos, *ACS Sustain. Chem. Eng.*, **1**, 1545 (2013).
16. Y. Wang, T. Du, L. Zhou, Y. Song, S. Che and X. Fang, *Korean J. Chem. Eng.*, **35**, 709 (2018).
17. D. Pathania, S. Sharma and P. Singh, *Arab. J. Chem.*, **10**, S1445 (2017).
18. B. Kok, K. Tan, M. Vakili, B. Horri, P. E. Poh, A. Z. Abdullah and B. Salamatinia, *Sep. Purif. Technol.*, **150**, 229 (2015).
19. H. Mirzazadeh and M. Lashanizadegan, *Korean J. Chem. Eng.*, **35**, 684 (2018).
20. S. Adhikari, S. Mandal, D. Sarkar, D.-H. Kim and G. Madras, *Appl. Surf. Sci.*, **420**, 472 (2017).
21. J. Li, S. Sun, R. Chen, T. Zhang, B. Ren, D. D. Dionysiou, Z. Wu, X. Liu and M. Ye, *Environ. Sci. Pollut. Res. Int.*, **24**, 9556 (2017).
22. J. He, J. Wang, Y. Liu, Z. Mirza, C. Zhao and W. Xiao, *Ceram. Int.*, **41**, 8028 (2015).
23. Y. Yu, Z. Hu, Y. Zhang and H. Gao, *RSC Adv.*, **6**, 18577 (2016).
24. K. Shen, M. A. Gondal, A. A. Al-Saadi, L. Li, X. Chang and Q. Xu, *Res. Chem. Intermed.*, **41**, 2753 (2015).
25. M. Heidarizad and S. S. Şengör, *J. Mol. Liq.*, **224**, 607 (2016).
26. F. Mian, G. Bottaro, M. Rancan, L. Pezzato, V. Gombac, P. Fornasiero and L. Armelao, *ACS Omega*, **2**, 6298 (2017).
27. S.-M. Park and C. Nam, *Ceram. Int.*, **43**, 17022 (2017).

28. A. Staerz, U. Weimar and N. Barsan, *Sensors (Basel, Switzerland)*, **16**, 1815 (2016).
29. J.-H. Choi, S.-K. Kim and Y.-C. Bak, *Korean J. Chem. Eng.*, **18**, 719 (2001).
30. S. Shamaila, A. K. L. Sajjad, F. Chen and J. Zhang, *J. Colloid Interface Sci.*, **356**, 465 (2011).
31. M. Fojtu, W. Z. Teo and M. Pumera, *Environ. Sci.: Nano*, **4**, 1617 (2017).
32. R. Halvaeifard and S. Sharifnia, *Korean J. Chem. Eng.*, **35**, 770 (2018).
33. S. A. McCarthy, R. Ratkic, F. Purcell-Milton, T. S. Perova and Y. K. Gun'ko, *Sci. Reps.*, **8**, 2860 (2018).
34. S. Adhikari and D. Sarkar, *Electrochim. Acta*, **138**, 115 (2014).
35. H. Wu, X. Ding, W. Li, C. Ren and H. Yang, *J. Mater. Sci.: Mater. Electron.*, **28**, 18542 (2017).
36. Z. S. Seddigi, M. Gondal, U. Baig, S. A. Ahmed, M. Abdulaziz, E. Danish, M. Khaled and A. Lais, *PloS ONE*, **12**(2), 1 (2017).
37. N. Malusi Mkhize, B. Sithole and M. Ntunka, *J. Wood Chem. Technol.*, **35**, 374 (2015).
38. Q. Fan, J. Liu, Y. Yu and S. Zuo, *RSC Adv.*, **4**, 61877 (2014).
39. X. Gao, W. Peng, G. Tang, Q. Guo and Y. Luo, *J. Alloys Compd.*, **757**, 455 (2018).
40. Y. Cai, D. Li, J. Sun, M. Chen, Y. Li, Z. Zou, H. Zhang, H. Xu and D. Xia, *Appl. Surf. Sci.*, **439**, 697 (2018).
41. S. Mandal, T. Padhi and R. K. Patel, *J. Hazard. Mater.*, **192**, 899 (2011).
42. D. Robati, *J. Nanostructure Chem.*, **3**, 55 (2013).
43. T. S. Natarajan, H. C. Bajaj and R. J. Tayade, *J. Colloid Interface Sci.*, **433**, 104 (2014).
44. K. Syam and J. Pethaiyan, *Eur. J. Inorg. Chem.*, **2015**, 4260 (2015).
45. Y. Bessekhouad, D. Robert, J. V. Weber and N. Chaoui, *J. Photochem. Photobio. A: Chem.*, **167**, 49 (2004).
46. S. A. Singh and G. Madras, *Sep. Purif. Technol.*, **105**, 79 (2013).
47. J. Song, Q. Fan, W. Zhu, R. Wang and Z. Dong, *Mater. Lett.*, **165**, 14 (2016).
48. Q. Zhao, Y. Xing, Z. Liu, J. Ouyang and C. Du, *Nanoscale Res. Let.*, **13**, 69 (2018).
49. Z. Ding, W. Wang, Y. Zhang, F. Li and J. P. Liu, *J. Alloys Compd.*, **640**, 362 (2015).